3D fatigue fracture modeling by isogeometric boundary element methods

*Xuan Peng[1], Elena Atroshchenko[2], Pierre Kerfriden[1] and Stéphane P. A. Bordas[3, 1, 4]

[1]Institute of Mechanics Materials and Advanced Manufacturing, Cardiff University, CF24 3AA, UK
[2]Department of Mechanical Engineering, University of Chile, Santiago, 8370448, Chile
[3]Institute for Computational Engineering, Université du Luxembourg, 6 rue Richard Coudenhove-Kalergi,
L-1359, Luxembourg
[4]School of Mechanical and Chemical Engineering, The University of Western Australia (M050), WA 6009,
Australia

PengX2@cardiff.ac.uk

ABSTRACT

The isogeometric boundary element method (IGABEM) based on NURBS is adopted to model fracture problem in 3D. The NURBS basis functions are used in both crack representation and physical quantity approximation. A stable quadrature scheme for singular integration is proposed to enhance the robustness of the method in dealing with highly distorted element. An algorithm is outlined and validated to be stable for fatigue crack growth, thanks to the smoothness not only in crack geometry but also in stress/SIFs solution brought by IGABEM.

Key Words: Isogeometric analysis; NURBS; Linear elastic fracture; Boundary element method; Crack growth

1. Introduction

The fracture modeling by the boundary element method (BEM) exhibits more advantages than by FEM in terms of mesh/re-mesh efforts as only the boundary discretization is required in BEM in order to approximate the quantity of interest. When cracks evolve, only the boundary surfaces are updated instead of re-generating the volume mesh.

The isogeometric analysis (IGA) was first introduced by Hughes *et al* [1]. The basic idea of IGA is to use the same spline basis functions to represent the CAD geometries and approximate the physical quantities of interest. And the investigation on the joint of IGA and BEM (IGABEM) [2] has increasingly drawn attention recently since only the boundary representation of the geometry is required in IGABEM, which facilitates the integration of design and analysis.

The advantages of the application for fracture based on the IGA framework can be concluded as:

(1) The higher-order continuity of spline basis functions improves the accuracy of the stress field near the crack front which is crucial to fracture analysis and the degrees of freedom is reduced compared to the C^0 Lagrange basis;
(2) The curvature, tangential and normal vectors are exactly retained and evolved for the crack growth thanks to the exact representation of the curved cracks;
(3) The local crack tip (front) system can be constructed directly based on the spline-based curve or surface-represented cracks, which helps to accurately evaluate the fracture parameters;
(4) The concept of integration through design to analysis facilities the mechanical/structural design based on the fatigue fracture analysis.

2. Boundary integral equations (BIE) for crack modeling

Consider an arbitrary domain Ω which contains a crack. The boundary of the domain $\partial\Omega = S \cup S_{c^+} \cup S_{c^-}$, where S is composed of S_u where Dirichlet boundary conditions are prescribed (known displacements $\bar{\mathbf{u}}$), S_t where Neumann boundary conditions are prescribed (known tractions $\bar{\mathbf{t}}$). The displacement BIE

(Equation (1)) is used on one face (S_{c+}) and on the rest of the boundary S. The traction BIE (Equation (2)) is used on the other crack face (S_{c-}).

$$c_{ij}(\mathbf{s}^+)u_j(\mathbf{s}^+) + c_{ij}(\mathbf{s}_m^-)u_j(\mathbf{s}^+) = \int_S U_{ij}(\mathbf{s}^+,\mathbf{x})t_j(\mathbf{x})\mathrm{d}S(\mathbf{x}) - \int_S T_{ij}(\mathbf{s}^+,\mathbf{x})u_j(\mathbf{x})\mathrm{d}S(\mathbf{x})$$

$$- \oint_{S_{c+}} T_{ij}(\mathbf{s}^+,\mathbf{x}^+)u_j(\mathbf{x}^+)\mathrm{d}S(\mathbf{x}) - \oint_{S_{c-}} T_{ij}(\mathbf{s}_m^-,\mathbf{x}^-)u_j(\mathbf{x}^-)\mathrm{d}S(\mathbf{x}) \tag{1}$$

$$+ \int_{S_{c+}} U_{ij}(\mathbf{s}^+,\mathbf{x}^+)t_j(\mathbf{x}^+)\mathrm{d}S(\mathbf{x}) + \int_{S_{c-}} U_{ij}(\mathbf{s}_m^-,\mathbf{x}^-)t_j(\mathbf{x}^-)\mathrm{d}S(\mathbf{x}),$$

$$c_{ij}(\mathbf{s}^-)t_j(\mathbf{s}^-) + c_{ij}(\mathbf{s}_m^+)t_j(\mathbf{s}^-) = \int_S K_{ij}(\mathbf{s}^-,\mathbf{x})t_j(\mathbf{x})\mathrm{d}S(\mathbf{x}) - \int_S H_{ij}(\mathbf{s}^-,\mathbf{x})u_j(\mathbf{x})\mathrm{d}S(\mathbf{x})$$

$$- \oint\!\!\!= _{S_{c-}} H_{ij}(\mathbf{s}^-,\mathbf{x}^-)u_j(\mathbf{x}^-)\mathrm{d}S(\mathbf{x}) + \oint\!\!\!= _{S_{c+}} H_{ij}(\mathbf{s}_m^+,\mathbf{x}^+)u_j(\mathbf{x}^+)\mathrm{d}S(\mathbf{x}) \tag{2}$$

$$+ \oint_{S_{c-}} K_{ij}(\mathbf{s}^-,\mathbf{x}^-)t_j(\mathbf{x}^-)\mathrm{d}S(\mathbf{x}) - \oint_{S_{c+}} K_{ij}(\mathbf{s}_m^+,\mathbf{x}^-)t_j(\mathbf{x}^+)\mathrm{d}S(\mathbf{x}),$$

where the U_{ij}, T_{ij} are called fundamental solutions, and

$$H_{ij}(\mathbf{s},\mathbf{x}) = E_{ikpq}\frac{\partial T_{pj}(\mathbf{s},\mathbf{x})}{\partial s_q}n_k(\mathbf{s}), \quad K_{ij}(\mathbf{s},\mathbf{x}) = E_{ikpq}\frac{\partial U_{pj}(\mathbf{s},\mathbf{x})}{\partial s_q}n_k(\mathbf{s}), \tag{3}$$

where $\oint$ denotes the integral is interpreted in the *Cauchy Principal Value* sense and $\oint\!\!\!=$ denotes the *Hadamard Finite Part* integral. $\mathbf{s}_m^-$ denotes the mirror point of $\mathbf{s}^+$ on S_{c-}, which means $\mathbf{s}_m^-$ and $\mathbf{s}^-$ share the same physical and parametric coordinates but their normal vectors are opposite. The last two terms of both equations and left hand side of Equation (2) are omitted due to the traction-free crack.

3. Singularity subtraction technique (SST) for singular integrals

For the hyper-singular integral

$$I = \lim_{\varepsilon \to 0} \int_0^{2\pi} \int_{\alpha(\varepsilon,\theta)}^{\hat{\rho}(\theta)} H(\rho,\theta)R(\rho,\theta)\bar{J}(\rho,\theta)\rho\,\mathrm{d}\rho\mathrm{d}\theta, \tag{4}$$

where H is the hyper-singular kernel, R is the NURBS basis function and $\bar{J}$ is the Jacobi transformation from parent space to physical space. The integrand $F(\rho,\theta) = H(\rho,\theta)R(\rho,\theta)\bar{J}(\rho,\theta)\rho$ is expanded as:

$$F(\rho,\theta) = \frac{F_{-2}(\theta)}{\rho^2} + \frac{F_{-1}(\theta)}{\rho} + F_0(\theta) + F_1(\theta)\rho + F_2(\theta)\rho^2 + \cdots = \sum_{i=-1}^{\infty} F_i(\theta)\rho^i. \tag{5}$$

The singularity can be represented explicitly with respect to the parametric distance between the source point and field point ρ. Then the singular terms are subtracted from the integrand, leaving the remaining to be regular for which regular Gaussian rule is applied. the subtracted terms are added back semi-analytically, resulting in:

$$I = I_1 + I_2,$$

$$I_1 = \int_0^{2\pi} \int_0^{\hat{\rho}(\theta)} \left[F(\rho,\theta) - \frac{F_{-2}(\theta)}{\rho^2} - \frac{F_{-1}(\theta)}{\rho}\right]\mathrm{d}\rho\mathrm{d}\theta, \tag{6}$$

$$I_2 = \int_0^{2\pi} I_{-1}(\theta)\ln\frac{\hat{\rho}(\theta)}{\beta(\theta)}\mathrm{d}\theta - \int_0^{2\pi} I_{-2}(\theta)\left[\frac{\gamma(\theta)}{\beta^2(\theta)} + \frac{1}{\hat{\rho}(\theta)}\right]\mathrm{d}\theta,$$

where I_1 is regular and I_2 are regular line integrals, Both can be applied with Gaussian quadrature rule. The evaluation of $\alpha(\varepsilon,\theta)$, $\beta(\theta)$ and $\gamma(\theta)$ as well as the limiting process can be referred in [3].
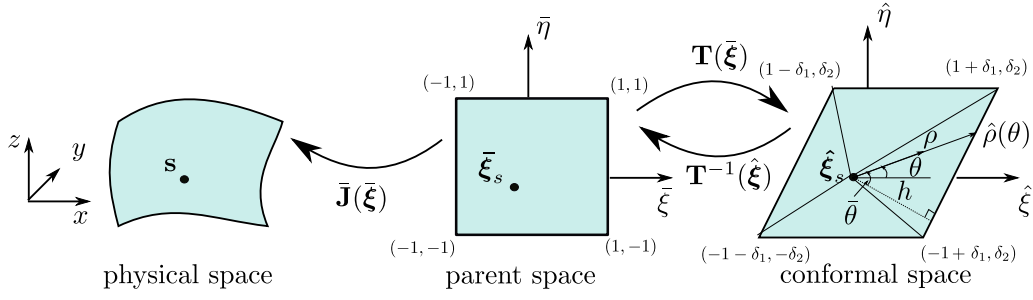
Figure 1: Transformation between coordinate system for SST. The nodal coordinates $\hat{\xi}^I$ are obtained through bilinear interpolation from $(\bar{\xi}, \bar{\eta})$ to the new parametric space $(\hat{\xi}, \hat{\eta})$ for the quadrilateral element in conformal space

A conformal mapping is proposed to enhance singular integration for distorted elements. The curvilinear basis vectors $\mathbf{m}_i^s = \mathbf{m}_i|_{\bar{\xi}=\bar{\xi}_s}, (i = 1, 2)$ and are calculated as:

$$\mathbf{m}_1 = \left[\frac{\partial x}{\partial \bar{\xi}}, \frac{\partial y}{\partial \bar{\xi}}, \frac{\partial z}{\partial \bar{\xi}}\right],$$
$$\mathbf{m}_2 = \left[\frac{\partial x}{\partial \bar{\eta}}, \frac{\partial y}{\partial \bar{\eta}}, \frac{\partial z}{\partial \bar{\eta}}\right]. \tag{7}$$

We introduces two parameters $\lambda = |\mathbf{m}_1^s|/|\mathbf{m}_2^s|$, $\cos\psi = \mathbf{m}_1^s \cdot \mathbf{m}_2^s/|\mathbf{m}_1^s||\mathbf{m}_2^s|$. The conformal mapping from the parent space $(\bar{\xi}, \bar{\eta})$ to a new parametric space $(\hat{\xi}, \hat{\eta})$ can be constructed where the two curvilinear basis vectors in the new parametric space are orthogonal and have identical length. The Jacobian transformation matrix $\mathbf{T}$ from $\bar{\xi} = (\bar{\xi}, \bar{\eta})$ to a new parametric space $\hat{\xi} = (\hat{\xi}, \hat{\eta})$ is

$$\mathbf{T} = \begin{bmatrix} 1 & \delta_1 \\ 0 & \delta_2 \end{bmatrix}, \text{ so that } \hat{\xi} = \mathbf{T}\bar{\xi}, \tag{8}$$

where $\delta_1 = \cos\psi/\lambda$, $\delta_2 = \sin\psi/\lambda$. Figure 1 illustrates the transformation for singular integration. Now the SST is applied in the conformal space.
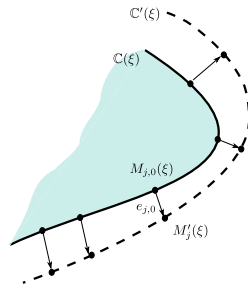

Figure 2: Crack front updating. $\mathbb{C}(\xi)$ is the old crack front curve, $\mathbb{C}'(\xi)$ is the new crack front curve after crack advance

4. Crack growth

In the present work, we use NURBS patches to discretize the crack surfaces. The Paris law is used to calculate the crack advance. A crack surface updating algorithm is outlined to perform the crack growth as in Table 1.

5. Numerical examples

Figure 3(a) shows the convergence study on the relative error in the L_2 norm crack opening displacement (COD) for the penny crack problem with inclination angle $\varphi = 0$. It can be seen that degree elevation

---
Algorithm 1 Crack front updating algorithm

Data: old crack front curve $\mathbb{C}(\xi)$; sample points M_j; new positions of sample points M'_j
Result: new crack front curve that passes through all M'_j, see Figure 2
$t = 0$;
$tol = 1.e - 4$;
$e_{j,0} = \overrightarrow{M_{j,0}M'_j}$;   //the initial error vector
while $\|e_t\| > tol$ **do**
$\quad | \quad t = t + 1$;
$\quad | \quad m_{i,t} = \frac{1}{N}\sum_{j=0}^{N-1} f_{ij}e_{j,t-1}$;   //the motion vector at t-th step
$\quad | \quad P_{i,t} = P_{i,t-1} + m_{i,t}$;   //the new point on the crack front at t-th step
$\quad | \quad e_{j,t} = e_{j,t-1} - \frac{1}{N}\sum_{k=0}^{N-1}\sum_{i=0}^{n-1} R_{ij}f_{ik}e_{k,t-1}$;   //the error vector at t-th step

end
---

from 2 to 3 improves accuracy. Yet, the convergence rate (oc) keeps almost the same value ($oc = 1$). The deterioated oc is due to the physical singularity along the crack front. Figure 3(b) shows the stress intensity factors (SIFs) for the sample points on the crack front for the penny crack problem with $\varphi = \pi/6$. It can be observed that the numerical SIFs agrees well with the analytical solution. Figure 4 presents the fatigue crack growth for inclined elliptical crack.
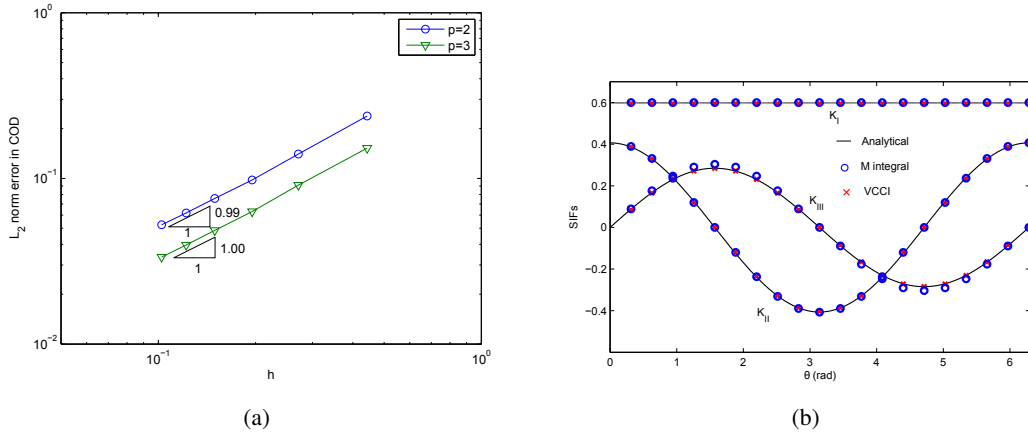

(a)   (b)

Figure 3: (a) The relative error in the L_2 norm of COD for penny-shaped crack by uniform mesh refinement in parametric space.; (b) Stress intensity factors for penny crack with inclination angle $\varphi = \pi/6$, θ is the direction angle for the sample points along the crack front

6. Conclusions

The formulation and implementation of isogeometric boundary element methods (IGABEM) for simulating 3D fatigue fracture problem are outlined in this paper. The same NURBS basis functions are used for the discretization of geometry/crack and the approximation of displacement/traction in the isogeometric framework. The highlights of this work include: (1) The proposed singular integration scheme can preserve the quadrature accuracy for highly distorted elements which exist commonly in IGA; (2) The local crack tip system is setup naturally and uniquely thanks to the NURBS representation of the crack surface. With the continuity in stress solution in BEM, the obtained SIFs along the crack front are smooth and accurate; (3) The proposed algorithm for crack propagation is validated to be stable, due to the smoothness in crack front geometry and numerical SIFs.

The future work will focus on the surface cracks problem, where the crack will have intersection with the body geometry.

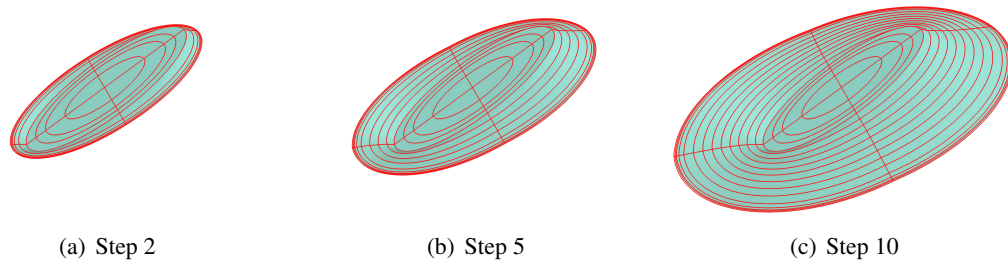| (a) Step 2 | (b) Step 5 | (c) Step 10 |

Figure 4: Fatigue crack growth simulation of an elliptical crack with inclination angle $\varphi = \pi/6$ modeled by the dual equations in a finite domain

References

[1] Hughes T J R, Cottrell J A, Bazilevs Y. Isogeometric analysis: CAD, finite elements, NURBS, exact geometry and mesh refinement. *Computer methods in applied mechanics and engineering*, 2005, 194(39): 4135-4195.

[2] Scott, M. A., Simpson, R. N., Evans, J. A., Lipton, S., Bordas, S. P., Hughes, T. J., Sederberg, T. W. (2013). Isogeometric boundary element analysis using unstructured T-splines. *Computer Methods in Applied Mechanics and Engineering*, 254, 197-221.

[3] Guiggiani M. Formulation and numerical treatment of boundary integral equations with hypersingular kernels. *Singular integrals in boundary element methods*, 1998: 85-124.